Title

Polyploidy in Xenopus lowers metabolic rate by decreasing total cell surface area.

Journal

Current Biology, 33(9)

Authors

Bartz, Julianne

Oaks, Gillian

Liu, Martin

et al.

Publication Date

2023-05-08

DOI

10.1016/j.cub.2023.03.071

Peer reviewed

HHS Public Access

Author manuscript

Curr Biol. Author manuscript; available in PMC 2024 May 08.

Published in final edited form as:

Curr Biol. 2023 May 08; 33(9): 1744–1752.e7. doi:10.1016/j.cub.2023.03.071.

Polyploidy in *Xenopus* lowers metabolic rate by decreasing total cell surface area

Clotilde Cadart[1,2,3,*], **Julianne Bartz**[1], **Gillian Oaks**[1], **Martin Ziyuan Liu**[1], **Rebecca Heald**[1,2,*]

[1]Department of Molecular and Cell Biology, University of California, Berkeley, Berkeley, CA 94720-3200, USA.

[2]Twitter: @rebeccaheald; @clotildecadart

[3]Lead contact

SUMMARY

Although polyploidization is frequent in development, cancer, and evolution, impacts on animal metabolism are poorly understood. In *Xenopus* frogs, the number of genome copies (ploidy) varies across species and can be manipulated within a species. Here we show that triploid tadpoles contain fewer, larger cells than diploids and consume oxygen at a lower rate. Drug treatments revealed that the major processes accounting for tadpole energy expenditure include cell proliferation, biosynthesis, and maintenance of plasma membrane potential. While inhibiting cell proliferation did not abolish the oxygen consumption difference between diploids and triploids, treatments that altered cellular biosynthesis or electrical potential did. Combining these results with a simple mathematical framework, we propose that the decrease in total cell surface area lowered production and activity of plasma membrane components including the Na^+/K^+ ATPase, reducing energy consumption in triploids. Comparison of *Xenopus* species that evolved through polyploidization revealed that metabolic differences emerged during development when cell size scaled with genome size. Thus, ploidy affects metabolism by altering the cell surface area to volume ratio in a multicellular organism.

Graphical Abstract

[*]Correspondence: bheald@berkeley.edu; clotilde.cadart@berkeley.edu.

AUTHOR CONTRIBUTIONS

Conceptualization: CC, RH; Experiments: CC, JB, GO, ML; Analysis & framework: CC; Funding acquisition: RH; Supervision: RH; Manuscript preparation: CC, RH

DECLARATION OF INTERESTS

Authors declare that they have no competing interests.

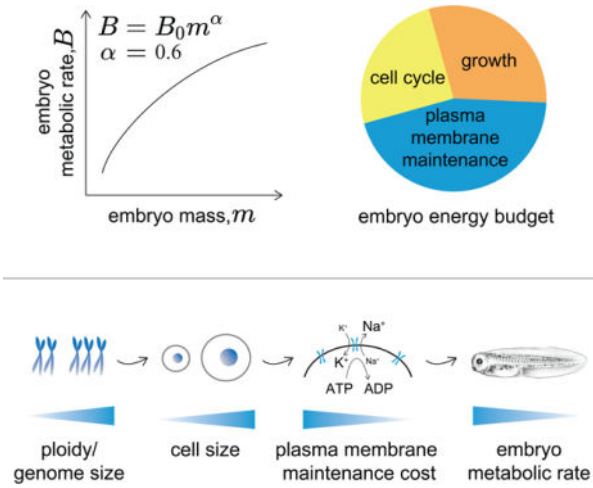

eTOC Blurb

Cadart *et al.* show that triploid *X. laevis* tadpoles have fewer, larger cells and a lower oxygen consumption rate than diploids due to reduced total cell surface area, which decreases energy required to maintain the plasma membrane. Comparing *Xenopus* species ranging 6-fold in ploidy reveals that metabolic rate scales with cell size, not genome size.

Keywords

polyploidy; cell size; metabolism; scaling; *Xenopus* ; Kleiber's law; energy budget

INTRODUCTION

An increase in genome copy number or ploidy is a central phenomenon in biology that occurs during the development of specific tissues[1], is frequently observed in tumorigenesis[2] and is a major driving force of speciation throughout evolution[3]. In these various contexts, the benefits of polyploidization are diverse, but one fundamental question is how ploidy impacts energy expenditure of the tissue, tumor, or organism.

Unlike for most animals, polyploidization can easily be induced at fertilization in frog and fish embryos, which develop normally[4,5]. Such artificially induced increases in ploidy have been observed to lower whole-body metabolic rate in both larvae and adults[6–9] and have been proposed to involve a ploidy-induced increase in cell size[10], but this has not been demonstrated experimentally.

Increased cell size is a ubiquitous consequence of polyploidization in yeast[11,12], vertebrate muscle cells[13], and fish[5,14,15] but little is known about how cellular metabolism is impacted[16]. In unicellular organisms, cellular respiration was shown to scale sublinearly with cell size[17], reminiscent of Kleiber's famous power-law connecting animal metabolic rate to body mass with a ¾ exponent[18]. Although theories are rife[19], knowledge of mechanisms by which cell size affects metabolism is limited. Recently, research on experimentally induced polyploid yeast[12] or animal cells[20] revealed decreased expression

of mitochondrial genomes, mRNA, and proteins with increased ploidy. Additionally, experiments in single animal cells revealed that mitochondrial membrane potential peaks at intermediate cell sizes[21] and age-induced cellular enlargement correlated with decreased mitochondria concentration in mouse hematopoietic stem cells[22]. Altogether, these results suggest that cellular metabolism, specifically oxygen consumption due to mitochondrial respiration, changes as a function of ploidy and cell size, but why this occurs is unknown[16]. Moreover, how ploidy changes impact metabolism of a tissue or whole organism is poorly understood.

To investigate the interplay between ploidy, cell size, and organismal metabolism, we established a quantitative framework to characterize how oxygen consumption rate relates to cellular energetic needs in *X. laevis* embryos and tadpoles of different ploidy. Using specific inhibitor treatments, we established an energy budget for embryogenesis and show that triploids containing fewer, larger cells than diploids possess a lower metabolic rate, independent of differences in cell proliferation. Inhibiting the Na^+/K^+ ATPase pump abolished the metabolic difference between diploids and triploids, suggesting that less energy is required to maintain plasma membrane potential in triploids due to the lower cell surface area to volume ratio. A simple mathematical framework recapitulated the reduction in energy costs associated with a lower cell surface area to volume ratio in triploids. Inhibiting mTOR signaling also erased the ploidy-dependent difference in metabolic rates, possibly due to downregulation of plasma membrane-associated protein and lipid synthesis in larger triploid cells. Crucially, we show that across *Xenopus* species of increasing ploidy, metabolic rate decreases only when cell size correlates with genome size[23], demonstrating that cell size, not genome size, is the key variable determining embryo metabolic rate.

RESULTS

Triploid *X. laevis* embryos have increased cell size and develop normally

To investigate the impact of ploidy on metabolism, we focused on frog embryos of the genus *Xenopus*, whose ploidy can be easily manipulated at fertilization[4], producing diploid and triploid embryos from the same clutch of eggs (Figure 1A–C). Triploid embryos accumulated mass similarly to diploids except for a transient ~5% decrease at day 3 post fertilization (p.f.) (Figure 1D and Table S1) and had comparable developmental and survival rates (Figure S1A and B). To measure cell size, we stained embryos at stages 33–34, 37–38, and 41 for cortical actin (Figure 1E) and quantified the area of multi-ciliated cells (Figure 1F) and goblet-like cells (Figure S1C) present in surface epithelia. At all these stages, triploids displayed an increase in cell area reflecting a linear relationship between spherical cell volume and ploidy (Figures 1F and S1C), consistent with previous findings in yeast[11,12] and fish[5,14]. Therefore, triploid *X. laevis* embryos provide a means to evaluate the effects of a 50% genome size and comparable cell size increase on metabolism in a normally developing vertebrate.

Metabolic rate scales sublinearly with increasing body mass during development

Metabolic rate B and body mass m are related across all animals by Kleiber's law[18]: $B = B_0 m^{\alpha}$ with an allometric exponent α value that is typically between 0.6 and 0.75 for

adult animals[24,25], but has not been characterized during development. Using a non-invasive detection system, we measured oxygen consumption rate (OCR), the most commonly used proxy for whole-organism metabolism[26], of single embryos in glass vials filled with water by recording oxygen consumption over 5–7 hours (Figures 2A and S2A–H). OCR measurement of more than 250 diploid embryos from day 2 to day 5 p.f. showed that metabolic rate increased with body mass following a power-law with a scaling exponent (a = 0.58 ± 0.02), consistent with Kleiber's law (Figure 2B, Methods, and Table S2). Thus, as in adults, allometric metabolic scaling occurs in early vertebrate development.

Embryo metabolic rate is 6% lower in triploids starting at the tadpole phase

We then compared the metabolic rates of diploid and triploids. To account for the mass-dependent increase in OCR and potential effects of embryonic development on energy expenditure patterns, measurements were binned by both animal mass and developmental stage (Figure 2C, Table S3). Consistent with Kleiber's law, mass-normalized OCR was lower for bins of higher mass due to the sublinear increase of metabolic rate with body size. At the late tailbud stage 33–34, around 46 hours post fertilization (h.p.f.), we observed no significant difference in mass-normalized OCR between diploids and triploids. However, by the early tadpole stage 41 (~72 h.p.f.), triploids displayed a 5.1% lower metabolic rate, a trend that persisted through later developmental stages up to day 5 (Figure S2I). Due to the ZZ/ZW sex determination mechanism of *X. laevis*, all triploids are female[27], and sex-specific differences in metabolic rate have been reported in vertebrates[28]. However, OCR measurements of male and female diploids at stage 41 showed no significant difference (Figure S2J). To probe the conservation of this ploidy-dependent OCR decrease, we repeated our measurements using the closely related species *X. borealis* and similarly observed that triploids possessed a lower metabolic rate compared to diploids at stage 41 (8.1%) (Figures 2C and S2K). Importantly, plotting OCR vs. body mass for diploid and triploid *X. laevis* tadpoles revealed no difference in the scaling exponent, but rather different normalization constants (Y-intercepts, diploids: B_0 = 0.0111 ± 0.0005, triploids: B_0 = 0.0106 ± 0.0005) (Figure 2D and Table S2). Therefore, beginning at the tadpole phase, both *X. laevis* and *X. borealis* triploids show an average 6% ± 0.01 decrease in metabolic rate compared to diploids (Figure S2K).

An embryo energy budget establishes the costs of proliferation, biosynthesis, and maintenance

To understand why whole-organism metabolic rate is reduced in triploids, we first sought to identify processes that contribute significantly to the embryo energy budget. Theoretical studies have proposed that organismal metabolism (B) can be partitioned into two main processes, growth and maintenance[29–33]. In multicellular organisms, attempts to experimentally relate whole-organism energy expenditure to empirical measurements of the cost of such processes have been limited. One notable exception is pioneering work in zebrafish embryos demonstrating that the pathways enabling synchronous cell divisions account for energy expenditure oscillations measured during the first hours of development[34]. Since proliferation and growth are often decoupled during development[35], we sought to distinguish the costs of proliferation, mass synthesis and maintenance by measuring OCR upon chemical inhibition of key regulators of each process. We focused

on diploid *X. laevis* embryos at stage 41, when a stable regime of mass-normalized OCR reduction with ploidy was apparent (Figure 2D).

To estimate the cost of proliferation, we measured OCR in diploids upon treatment with palbociclib, an inhibitor of Cdk4/6 and cell cycle progression[22]. OCR decreased in a dose-dependent fashion until beginning to plateau (Figure 3A), suggesting that most of the energy expenditure for cell cycle progression was abolished in the animals. Staining of phosphor-histone H3, a marker of mitosis (Figure 3B), confirmed that mitotic cell density was significantly reduced upon palbociclib treatment in the tail, one of the most rapidly growing tissues at stage 41[36] (Figure S3A), with 85% and 72% decreases at the tail base and tip, respectively (Figures 3C). Palbociclib treatment reduced OCR by 26 ± 1% compared to untreated diploids, suggesting that proliferation accounts for about one fourth of the energy budget of embryos at stage 41 (Figure 3D–E). To estimate the cost of mass synthesis, we blocked growth signaling using two inhibitors of the mTOR pathway, torin-1 and torkinib, which reduced OCR by 32 ± 3 % and 29 ± 3 %, respectively (Figures 3D and S3B), indicating that protein synthesis represents on average 30 ± 4 % of the embryo energy budget (Figure 3E). Finally, to estimate the cost of cellular maintenance, we considered the high energetic cost of the Na^+/K^+ ATPase pump[37,38] that maintains the plasma membrane potential and has been estimated to represent ~24 to 70% of cellular oxygen consumption depending on the cell type[39,40]. Inhibition of the Na^+/K^+ ATPase pump with ouabain[37] decreased OCR by 46 %, (Figures 3D, 3E and S3C–D). The sum of the experimentally estimated costs of proliferation, protein synthesis, and maintenance came close to 100% (102 ± 4 %), suggesting that our analysis accounted for the core energy budget of the embryo (Figures 3E, S3E, and S4A–B). Thus, at stage 41, maintenance cost represents nearly half of the embryo energy budget and is mostly accounted for by ion pump activity at the plasma membrane.

Energy expenditures associated with plasma membrane maintenance and mTOR pathway account for the lower whole-embryo metabolic rate in triploids

In addition to establishing an energy budget, inhibitor treatments allowed us to evaluate which processes contribute to the OCR decrease observed in triploids. The increase in cell size with ploidy at the same body mass indicated that triploid embryos contained fewer, larger cells than diploids and, if so, must have decreased rates of cell division. Indeed, at the peak of tail growth (stage 41, day 3 p.f.) mitotic cell density was significantly higher in diploid embryos (Figure 4A). However, ploidy-dependent differences in OCR persisted upon palbociclib treatment (Figure 4B) even though differences in mitotic cell density across ploidies were abolished (Figure S4C). Thus, differences in metabolic rate as a function of ploidy are not explained by altered rates of cell division and associated energy costs.

We next evaluated whether maintenance costs, which represented the largest fraction of the embryo energy budget, could explain the metabolic difference across ploidies. Ouabain treatment abolished the OCR difference between diploids and triploids, as did treatment with a low concentration of DMSO (0.1%), known to perturb membrane stability and ion pumps non-specifically[41,42] (Figure 4B and Table S4). Finally, we tested the contribution of cell growth signaling and found that torkinib treatment also eliminated the metabolic difference

between diploid and triploids (Figures 4B and S4D). Thus, energy expenditure related to the mTOR pathway and plasma membrane potential maintenance both contribute to the metabolic difference across ploidies. Importantly, ion gradient establishment via the Na^+/K^+ ATPase occurs at the plasma membrane and depends on cell surface area[16,19]. This suggests an intuitive cell size-dependent mechanism of energy expenditure reduction because triploid embryos have fewer larger cells, resulting in a correspondingly lower surface area to volume ratio.

A mathematical framework recapitulates the reduction in energy costs associated with a lower cell surface area to volume ratio in triploids

To explore whether surface area-dependent energetic costs associated with membrane maintenance could contribute to the 6% decrease in whole-embryo OCR, we adapted energy partition models[29–33] and wrote:

$$B = E_d \frac{dN_C}{dt} + \frac{E_s}{m_C}\frac{dm}{dt} + B_C N_C \quad (1)$$

where the metabolic rate B is determined by whole-embryo OCR and partitioned into three processes: (i) the cost E_d of cell division which increases with cell proliferation rate dN_C/dt, (ii) the cost E_s of synthesizing new units of mass m, normalized to the mass of a cell m_C that increases with biosynthesis rate dm/dt, and (iii) the cost of cellular maintenance which is the product of cellular metabolic rate B_C and the number of cells N_C (see details in the Methods). Our results suggest that cell proliferation cost does not change with ploidy while Na^+/K^+ ATPase activity, which represents a major part of maintenance cost and scales with surface area, does (Figure 4B). If maintenance costs scale primarily with cell surface area, which relates to cell volume (V_C) with an exponent of 2/3, and the total cell number scales inversely with ploidy due to the linear cell volume increase with ploidy ($N_C \sim 1/V_C \sim 1/P$) (Figure 1F), the relationship to ploidy P would be:

$$B_C N_C \sim P^{-1/3} \quad (2)$$

Combining with equation (1) and using the empirically measured fraction of energy allocated to cellular maintenance (46 ± 4 %, Figures 3E), the expected ratio of triploid to diploid metabolic rate equals 0.942 ± 0.005 (see SI), a value in remarkable agreement with our experimental measurement of 0.94 ± 0.02 (Figure S2K). Note that this estimate focuses on maintenance costs and specifically addresses how processes that scale with surface area such as membrane potential maintenance or synthesis of plasma membrane proteins and lipids can contribute to overall metabolism. It thus may not fully capture our observation that growth signaling inhibition also erases the metabolic difference (Figure 4B). Nevertheless, this approach provides a useful framework for understanding how an increase in cell size that results in a lower surface area to volume ratio contributes to reduced energy expenditure in polyploid animals. Importantly, maintenance costs that scale with cell volume and increase with ploidy following: $B_C \sim V_C \sim P$ are unlikely to contribute to an overall difference in metabolism with ploidy since the inverse relationship between cell number and cell volume -at constant body mass- dictates that the product $B_C N_C$ is constant (see SI).

Across three *Xenopus* species, metabolic rate correlates with cell size, not genome size

Polyploidization increases genome size and drives speciation among amphibians[43] and genome size has often been thought to negatively correlate with organismal variables such as developmental rate[43] or metabolic rate[44], but direct measurements across related species in a controlled experimental system are lacking. We wondered whether, similar to acute changes in ploidy within a species, evolutionary changes in ploidy across species led to mass-normalized differences in metabolic rates. We recently characterized size metrics in diploid (2N) *X. tropicalis*, allo-tetraploid (4N) *X. laevis*[45], and dodecaploid (12N) *X. longipes*[46] (Figure 5A), and showed that genome-to-cell size scaling across these species emerged late in development at stage 48 (day 7 p.f.)[23] (Figures 5B and S5A). We measured OCR before and after the onset of cell size scaling to determine whether differences in metabolic rate resulted directly from genome size changes or depended on cell size differences. Whereas *X. tropicalis* were too small in mass to compare until week 5 of development (Figure S5B), *X. longipes* embryos are similar in size to *X. laevis*. At days 3–4 p.f. (stage 41–45), when cell size did not yet scale with genome size, there was no statistically significant difference in OCR between *X. laevis* and *X. longipes* (Figure 5C). In contrast, after the onset of cell size scaling, comparison of animals overlapping in mass including 7–13 days old (stage 48–50) *X. longipes*, 6–8 days old *X. laevis*, and 26–46 days old (stage 50–52) *X. tropicalis* tadpoles revealed a negative trend between metabolic rate and cell size (Figure 5C and Table S5). This result indicates that, at least among closely related *Xenopus* species, cell size enlargement underlies the lower metabolic rate observed with increasing genome size[43,47] (Figure 5D).

DISCUSSION

In conclusion, *Xenopus* embryos display metabolic scaling with body mass during development consistent with Kleiber's law, but with a lower basal metabolic rate in triploids compared to diploids. An energy budget analysis revealed that proliferation, biosynthesis, and ATPase activity that maintains the plasma membrane potential largely account for the metabolic expenditure of embryos and tadpoles. Surprisingly, although cell proliferation rates are lower in triploids, this difference did not contribute to the ploidy-dependent metabolic decrease, while growth signaling pathways and plasma membrane maintenance did. Using a simple framework, we propose that the decrease in total cell surface area lowered production and activity of plasma membrane components including the Na^+/K^+ ATPase, reducing energy consumption in triploids. The comparison across three *Xenopus* species further demonstrated that increases in cell size, not genome size, drive a reduction in metabolic rate with ploidy and suggests a mechanism for the long observed correlations between genome size and organismal variables in evolutionary biology studies[43,47].

Whole-organism energetics depend on cell size

Cell size was hypothesized to mediate ploidy-dependent decreases in metabolic rate in fish by reducing cellular energy production capacity[8,10,14]. Here we show that energy consumption, not production, decreases with increasing cell size. Since triploid embryos contain fewer, larger cells and correspondingly lower total cell surface area, we propose that the energy required for maintaining the plasma membrane potential is reduced. This

is supported by our observation that inhibition of the Na^+/K^+ ATPase abolishes metabolic differences between diploids and triploids (Figure 4B) and by predictions based on a simple energy partitioning framework (Eq. 1, see Methods). Notably, our finding is in line with analysis of the first 10 hours of zebrafish embryo development, which showed that that energy expenditure increases with plasma membrane synthesis[48]. Future studies linking our findings to previous reports that mitochondrial respiratory proteins are under-expressed in polyploid yeast[12] or animal cells[20] will reveal how mitochondrial functions adapt to changing metabolic needs.

Our observation that mTOR inhibition also abolishes the ploidy-dependent metabolic difference raises the question of how biosynthesis changes with ploidy. Importantly, potential off-target effect of ouabain on growth regulation have been reported[37]. However, the wet mass increase observed upon ouabain treatment (Figure S3D) indicates that the drug primarily acts on ion transport and water intake, since the animals are not feeding. Future work may reveal whether there is general down-regulation of biosynthesis in triploids or a specific reduction in synthesis of plasma membrane-associated proteins and lipids, which like plasma membrane potential would scale with cell surface area. Previous reports showing that overall protein synthesis rate and cytoplasm density are constant as ploidy increases in single cells[49,50] support the latter hypothesis. Moreover, a possible explanation of the effect of torkinib (Figure 4B) is through inhibition of mTORC2[51], which is known to regulate production of lipids critical for plasma membrane synthesis[52,53].

The interplay between ploidy and metabolic pathways is developmentally-regulated

Decreased OCR in *X. laevis* triploids began at stage 41 and was robust through day 9 p.f. (Figures 3D and 5C), but this regime was preceded by a period when no difference in OCR was observed (stage 33–34, Figure 2C) even though cell size scaling was apparent (Figure 1F). These observations indicate developmentally-regulated changes in oxygen consumption pathways via mitochondria-independent[54] and -dependent pathways, motivating investigation of the metabolic pathways fueling development beyond the initial stages studied so far[55]. We predict that organ morphogenesis, such as the emergence of a functional pronephros that occurs just prior to the tadpole phase[56] and relies heavily on ionic pumps for osmolarity regulation[57], may shift the energy budget of embryos. How ploidy affects the interplay between metabolic pathways and embryo morphogenesis is thus an important area for future research.

Xenopus embryos provide a tractable system to bridge the gap between cellular and organismal physiology

Our findings highlight the value of investigating metabolic effects of cell size in the context of a multicellular organism or tissue. While there have been recent advances in theories of metabolic scaling[58] and cellular energetics[59,60], our work establishes quantitative approaches in a vertebrate system to bridge the gap between ploidy, cellular, and organismal metabolism and may have important implications in understanding metabolic constraints on genome size evolution[3,43]. Additionally, whether cell size increases characteristic of many cancers impact the energy budget of tumors may reveal novel insight into the benefits of polyploidization during tumor evolution[61,62].

STAR METHODS

RESOURCE AVAILABILITY

Lead Contact—Further information and requests for resources and reagents should be directed to and will be fulfilled by the lead contact, Clotilde Cadart, clotilde.cadart@berkeley.edu.

Materials Availability—All materials are available upon request. In general, antibodies are available for sharing.

Data and Code Availability—OCR measurement data reported in this paper will be shared by the lead contact upon request.

This paper does not report original code.

Any additional information required to reanalyze the data reported in this paper is available from the lead contact upon request.

EXPERIMENTAL MODEL AND SUBJECT DETAILS

Frog care—All frogs were used and maintained following standard protocols established by the UC Berkeley Animal Care and Use Committee and approved in our Animal Use Protocol. Mature *X. laevis, X. tropicalis* and *X. borealis* were obtained from Nasco (Fort Atkinson, WI) or the National *Xenopus* Resource (Woods Hole, MA). *X. longipes* were a kind gift from California Academy of Sciences (San Francisco, CA). All adult frogs were housed in a recirculating tank system with regularly monitored temperature and water quality. *X. laevis* and *X. borealis* were housed at 20–23°C, *X. tropicalis* at 23–26°C and *X. longipes* at 19–21°C. All animals were fed Nasco frog brittle.

X. laevis, X. tropicalis, and *X. borealis* females were ovulated with no harm to the animals with a minimum 4-months rest interval. To obtain testes for *in vitro* fertilizations (*X. laevis, X. tropicalis, X. borealis)*, males were euthanized by over-anesthesia through immersion in 0.05% benzocaine in double-distilled water (ddH_2O) prior to dissection. Carcasses were frozen at −20°C. Tadpoles used for experiments were euthanized similarly prior to fixation.

Natural matings were stimulated in *X. longipes* with no harm to males or females with a 6 to 12-months rest interval.

METHODS DETAILS

In vitro fertilization of *X. laevis, X. tropicalis* and *X. borealis*

The protocol for *in vitro* fertilizations was detailed previously[63]. For *X. laevis*, females were primed with 100 U of pregnant mare serum gonadotropin (PMSG, Calbiochem, #367222), at least 48 hr before boosting. The day before the planned experiment (14–16 hr before), females were boosted with 500 U of human Chorionic Gonadotropin (hCG) (Sigma #CG10) and kept at 16°C overnight in 1X MMR (1X MMR: 100 mM NaCl, 2 mM KCl, 2 mM $CaCl_2$, 1 mM $MgSO_4$, 0.1 mM EDTA, 5 mM HEPES-NaOH pH 7.6). *X. borealis* females were primed with 60 U of PMSG at least 48 hr before boosting with 300 U hCG 14–16 hr

before the fertilization and kept at 16°C in dionized water (diH_2O). *X. tropicalis* females were primed with 10 U hCG 14–16 hr before priming, kept at room temperature in diH_2O and boosted with 250 U the morning of the experiment. To obtain testes, males were euthanized by over-anesthesia through immersion in 0.05% benzocaine in ddH_2O. Testes were then dissected and kept up to a week at 4°C in 1X MR (100 mM NaCl, 1.8 mM KCl, 1 mM $MgCl_2$, 5 mM HEPES-NaOH pH 7.6 in ddH_2O) for *X. laevis* and *X. borealis* or placed in a solution of 0.2% BSA (Bovine Serum Albumin) in 1X MBS (1X MBS: 88 mM NaCl, 1.006 mM KCl, 2.49 mM $NaHCO_3$, 0.998 mM $MgSO_4$, 5 mM HEPES-NaOH pH 7.8) and used the same day for *X. tropicalis*. Once they started laying eggs, females were gently squeezed atop a petri dish (60 mm diameter) coated with 1.5% agarose in 1/10X MMR. Each dish of eggs was fertilized with a testis solution obtained by transferring a small piece of testis (~1/4 for *X. laevis* or *X. borealis*, ~1/2 for *X. tropicalis)* in 1 mL ddH_2O *(X. laevis* or *X. borealis)* or 0.5 mL 0.2% BSA in 1X MBS *(X. tropicalis)* in a 1.5 mL Eppendorf tube and crushing it using a plastic pestle. Eggs were gently swirled until they formed a monolayer at the bottom of the dish to ensure that all eggs came into contact with the testis solution, then dishes were slightly tilted to ensure immersion of all eggs and incubated for 10 min (*X. laevis* and *X. borealis)* or 5 min *(X. tropicalis)*. After this incubation time, eggs were covered with 1/10X MMR *(X. laevis* and *X. borealis)* or ddH_2O for 10 min, then 1/10X MMR *(X. tropicalis)*. To obtain triploid embryos, 1/10X MMR was kept at 4°C at least 2 hr before the fertilization, then, exactly 13 min post fertilization (m.p.f.) (*X. laevis)* or 10 m.p.f *(X. borealis)*, the media covering the eggs was quickly replaced with ice-cold 1/10X MMR and the dish was placed in a larger dish filled with ice-cold 1/10X MMR in an ice bucket for 15 min (*X. laevis, X. borealis)*. At the end of the cold shock, the media was quickly replaced with room-temperature 1/10X MMR and the petri dish was left to re-equilibrate. To ensure fast temperature-shift of the dishes, petri dishes with eggs intended to be triploids were not coated with agarose. At least 20 m.p.f. (diploid eggs) or 10 min after the cold shock (triploid eggs), fertilized eggs were de-jellied by incubating for ~5–8 min in freshly prepared de-jellying solution (3% L-cysteine in 1/10X MMR-NaOH, pH 7.8). As soon as the jelly coat was dissolved, eggs were washed at least 4 times with 1/10X MMR. At stages 2–3, fertilized eggs were sorted to remove all the unfertilized eggs and incubated at 24°C.

Natural mating of *X. longipes*

X. longipes males and females were injected with a priming dose of 75 U hCG the evening (~4 PM) before the planned mating day and kept at room temperature in separate tanks containing 1 X MMR in diH_2O. 10–11 hr later, the morning of the mating day (~3 AM), females were injected with a boosting dose of 200 U hCG. Amplexus typically started 6–8 hr later and eggs were collected in batches approximately every hour. Embryos were de-jellied and kept at 24°C as with other *Xenopus* species embryos.

Staging of *Xenopus* embryos

Embryos were staged according to the Nieuwkoop and Faber development table[64]. For stages 41 or older, tadpoles were transiently anesthetized by adding benzocaine to a final concentration of 0.008‰. This allowed manipulation of the embryos by turning them upside down using a hair tool and checking the number of gut loops, which is crucial for staging

at stages 41–48. Benzocaine was then rinsed off and tadpoles typically recovered and started swimming again within 10 min.

Maintenance of *Xenopus* embryos

On day 1 p.f. (post fertilization), embryos were transferred to larger dishes (100 mm diameter × 15 mm high). Dead or lysed embryos were removed and 1/10X MMR was changed ~2–3 times a day. To avoid potential sources of noise in embryo growth arising from variations in embryo density, *X. laevis* embryos were kept at 60 embryos or tadpoles in 60 mL 1/10X MMR per dish from day 1 onwards. For experiments on late-stage tadpoles in Figure 5 and S5B–C (day 7 or later), tadpoles were transferred to large containers with 2 L (week 2–3) or 4 L (week 4–7) diH_2O and tanks were kept in the lab at room temperature with a dark/light cycle of ~10/14 hr. Beginning on the morning of day 5, all tadpoles were fed everyday *ad libitum* with the light phase of decanted Sera Micron 5 mg/mL (Sera #00720). Sera micron was decanted because the heavier, larger flakes tended to choke young tadpoles.

Metaphase spreads

The protocol was adapted from a procedure kindly shared by the Harland lab. To perform metaphase spreads, 10–12 embryos at the tailbud stage (stage 26–34) were euthanized in 0.01‰ benzocaine in 1/10X MMR. The dorsal halves of the tadpoles were then dissected, removing as much of the yolky ventral portion as possible. Dorsal halves were incubated in colchicine (Sigma, #C9754) 1.2 mg/mL in 1/10X MMR for 1.5 hr (the stock was made fresh each time at 40 mg/mL in ddH_2O), then incubated in ddH_2O for 20 min, transferred to 0.5 mL Eppendorf tubes and incubated in 200 μL of 60% glacial acetic acid in ddH_2O for 5 min. Each dorsal half was gently transferred with a wide bore 200 μL pipette to a positively-charged glass slide (e.g., Fisherbrand, #12550400). Up to two dorsal halves per glass slides were placed on each glass slide, separated enough that the tissue would not mix once spread out. Excess liquid was blotted away if necessary and a large coverslip (e.g. VWR, 24 × 60 mm, No. 1.5, #48393–251) was put on top of the dorsal halves. To spread the chromosomes, a lead brick was placed on top of the glass slide protected by a paper towel for 5 min. When placing or removing the paper towel and lead brick, extra care was taken to prevent the coverslip from sliding (which otherwise would give metaphase spreads that were hard to quantify). The glass slide and coverslip were then put on dry ice for 5 min. Quickly after removal from the dry ice, the coverslip was detached from the glass slide using a razor blade to gently pry up by the edge of the coverslip from the frozen slide. Once the coverslip was removed, the metaphase spread was left to dry for 1–3 min. Once dry, the slide was mounted by putting a drop of Vectashield antifade mounting medium (Vector Laboratories, #H-1000–10) with Hoechst 0.1 mg/mL, covered with a coverslip (e.g. Thomas Brand, 22 × 22 mm No. 1.5 #1169W10) and sealed with nail polish. Slides were then stored in a box protected from light at 4°C until imaging.

Mass measurements

Mass measurements were performed using the Mettler Toledo Excellence XSR Analytical Balance with a 0.01 mg readability (#XSR105DU). One by one, each tadpole was transferred onto a glass coverslip, excess water was removed using a pipette and blotting

with kimwipes (Kimberley-Clark #34120). Rapidly after the measurement, the tadpole was placed back into water and, if needed, used for further analyses (e.g., proliferation assay after palbociclib treatment, Figure S4C).

Survival and developmental curves

For the survival and developmental curves (Figure S1A–B), three 60-mm diameter dishes with 30 embryos per ploidy and clutch were made on day 0 and survival was recorded 2 times per day during the first 3 days, then once per day for another 4 days (Figure S1A). For the developmental curve, to minimize the effect of temperature fluctuations on developmental rate, all dishes were placed on the middle shelf of the incubator and a rotation was established among the three dishes for each condition[65]. At each time point, the dish at the front of the shelf was taken out to assess the average stage in the dish, then placed at the back of the incubator, and so forth.

Oxygen consumption rate (OCR) measurements

Oxygen consumption rate measurements were performed using two Presens Sensor Dish Reader (SDR) v4 sets (Presens, #200001059) and 1 mL (day 1–2 p.f. embryos), 2 mL (Presens, #200001798) (day 3–5 p.f.) or 4 mL (Presens, #200001369) (day 7 or later p.f.) SensorVials which allowed measurement of up to 48 samples per experiment. For all the experiments, the system was placed in an incubator at 24°C with no light and measurements were made with one embryo per vial in ddH_2O. The day before the experiment, the SensorVials and two to four 100 mL bottles containing ~60 mL of ddH_2O were placed in a second 24°C incubator for temperature equilibration. The morning of the experiment, 24 diploid and 24 triploid embryos were staged and transferred into a large dish containing ddH_2O to rinse off the 1/10X MMR solution. To oxygenate the water, the bottles with ddH_2O were shaken vigorously for 60 sec, then gently tapped onto a table to help bring the bubbles to the surface. It was crucial not to introduce any bubbles in the vial. One by one, embryos were then transferred into a vial, the vial was filled to the brim with water, making sure that no bubbles were introduced, and the vial was sealed tightly with the cap and placed onto a transparent-bottom 24 multi-well plate. The incubator containing the SDR reader was opened only once, just briefly, to place the two multi-well plates and it was kept tightly closed for the rest of the experiment. O_2 levels were recorded every 5 min for 5–7 hr using the Presens software.

For each experiment, one of the vials contained no embryos in order to assess the time at which O_2 levels became stable (once the temperature had equilibrated). All timepoints acquired prior to this time were removed from the analysis (typically the first 2–3 hours, Figure S2A). Within each experiment, O_2 concentration in the blank vial fluctuated less than 0.4 ± 0.2% on average (Figure S2B) and temperature fluctuated less than 0.13 ± 0.06% on average (Figure S2C), thus indicating that measurements were made at near-equilibrium, with negligible temperature fluctuations. All experiments were performed in incubators set at 24°C and the temperature measured by the SDR device was on average 23.4°C, with only 0.92% fluctuations across all 66 experiments used for Figure 2B–D and 4 C–D (Figure S2D).

To calculate the rate of consumption of O_2 for each tadpole, a custom program in R was written to allow the user to select, for each curve, the first and last point between which to calculate a robust linear fit, using the 'lmrob' function with the MM-estimator algorithm[66] from the 'robustbase' package in R. During this process, the user could also exclude from the analysis any curve which presented too much noise (e.g., in case an air bubble caused a sudden drop in the curve). All the fits obtained were performed over at least 2 hr of continuous O_2 recording (Figure S2E), yielded R2 values that were higher than 0.90 (Figure S2F), and the calculated slopes (rates) were all statistically significant with p values smaller than 0.001 (Figure S2G).

Given the high variability in the OCR measured across individual tadpoles, we established the following controls and procedures to ensure robust results:

- Once we begun identifying a decrease in OCR in triploids compared with diploids at stage 41 (Figure 2C), we further confirmed the result by performing 3 blinded experiments in which the diploid and triploid dishes were randomly assigned a letter by another lab member. The ploidy was kept secret from the experimentalist until after the entire experiment was over, including tadpole staging, OCR recording, and data plotting and statistical analysis.
- During the analysis, the step at which the user could choose to remove a curve if it showed too much noise or abnormal variations or if the quality of the linear fit seemed unconvincing was done prior to matching the curve with the sample name and ploidy.
- A second step in the R analysis program, also prior to matching the measurement with the ploidy of the embryo, presented a plot showing OCR *vs.* embryo mass. This allowed identifying clear outliers (i.e., because of a mistake in the wet mass measurement or because of a problem on the linear fit which was always checked a second time in this case). However, most often, no outliers were identified at this step.
- All our results were obtained by comparing at least 3 clutches containing diploid and triploid embryos. The details of the number of clutches and individual embryos measured for each OCR result are reported in Tables S3–5.

Occasionally, a tadpole died during the measurement, halting a decrease of O_2 in the vial (Figure S2H). The absence of decrease was a clear indication that the potential contribution of bacteria to the measured oxygen consumption was negligible compared with that of embryos. Tadpoles that died during the experiment were excluded from the analysis.

PCR for sex determination

The protocol for PCR-based sex determination was kindly shared by Helen Willsey's lab (UCSF, CA) and was adapted from ref.[27]. Following OCR measurement, tadpoles were euthanized with 0.01‰ benzocaine in ddH_2O and the tail of each tadpole was sectioned, transferred to a 200 μL PCR tube, spun down to remove excess water and flash frozen at −80°C. To lyse the tails, 20 μL of 1X Phusion buffer (New England Biolabs, #E0553S) was added to each tube, tails were spun down briefly to ensure that

they were submerged and the following lysis program was started: boil at 95°C for 10 min, add 2.5 µL of 20 ng/mL Proteinase K (New England Biolabs, #P8107S) to each well, incubate at 55°C for 4 hr, boil again at 95°C for 10 min, store at 4°C. The PCR reaction was performed using the Phusion High-Fidelity PCR kit (New England Biolabs #E0553S) following the manufacturer's instructions. The following parameters were used: denaturation: 95°C, 30 sec; initiation: 98°C 10 sec; melting: 58°C, 30 sec; elongation: 72°C, 30 sec; extension: 72°C 10 min. Forward (AAAACCATGACCTCCCGGATAC) and reverse (TAGGGAGGGGTTTGGAGGTTC) primers amplified a 315 base-pair amplicon from the gene W3 whose presence is indicative of a female genotype. 100% of the triploids genotyped were positive for the gene W3 while the ratio of W3 positive tails in diploids were 11/23, 10/23 and 13/23 for the three clutches analyzed.

Phalloidin staining and immunofluorescence

The protocol for immunofluorescence combined with phalloidin staining was obtained from Helen Willsey's lab (UCSF, CA). The protocol for phospho-histone H3 staining was inspired by ref.[36]. 6–10 embryos of the desired stage were collected for each ploidy, fixed for 45 min in 4% PFA in PBS, then rinsed several times in PBS and kept at 4°C until use. Embryos were then permeabilized by incubating 3 × 20 min in PBS with 0.01% Triton x-100 (PBT), blocked for 1 hr at room temperature with PBT containing 10% goat serum. For phospho-histone H3 (pH3) staining for the tail proliferation assays, the following steps were performed: embryos were (a) incubated overnight at 4°C with 1:1000 mouse anti-histone H3 (phosphor Ser10), Abcam 14955, (b) rinsed 3 × 20 min in PBT, (c) incubated overnight at 4°C with 1:500 of the secondary antibody (goat-anti mouse coupled with AlexaFluor 488, Thermo Fisher Scientific), (d) rinsed again 3 × 10 min in PBS, (e) incubated with 0.01 mg/mL Hoechst for 20 min, (f) rinsed briefly with PBS, (g) mounted on slides in Vectashield just before imaging.

For cell size measurements, TMR-phalloidin 1X (Thermo Scientific #R415, stock at 400 X in DMSO according to the manufacturer's instructions) was added at step (c) or the experiment was done without steps (a)-(b). For cell size measurements at stage 48 (Figure 5B), phalloidin staining could not be used because it overwhelmingly stains the thick F-actin bundles along the tail muscle. We thus turned to immunofluorescence staining of ZO-1 to stain the cell membrane (Thermo Fisher Scientific #33–9100). The following protocol, adapted from ref.[67], was used. First, tadpoles were fixed for 1 hour in MAD fixative (2 parts methanol, 2 parts acetone, 1 part DMSO) then dehydrated in methanol and stored at 20°C. On day 1 of the staining procedure, the samples were: (a) gradually rehydrated in 0.5X SSC (1X SSC: 150 mM NaCl, 15 mM sodium citrate, pH 7), (b) bleached in bleaching solution (0.5X SSC solution containing 2%, H_2O_2 and 5% formamide) for 2–3 hr under light, (c) washed 3 × 10 min in PBT-BSA (PBT containing 2 mg/mL BSA), (d) blocked in PBT-BSA supplemented with 10% goat serum and 5% DMSO for 1–3 hr and finally (e) incubated at 4°C overnight in 300 µL of primary antibodies (ZO-1 at 1:250). The second day of the staining, samples were rinsed 4 × 2 hr in PBT then incubated overnight in PBT supplemented with 1:500 goat anti-mouse secondary antibody coupled to Alexa Fluor 488. On day 3, tadpoles were washed 4 × 2 hr in PBT and gradually dehydrated in methanol.

Embryos were then cleared in Murray's clearing medium (2 parts Benzyl Benzoate, 1 part Benzyl Alcohol).

Drug treatments

For each drug, the working concentration was determined in two steps. First, 5 embryos were incubated in 10 mL of increasing doses of each drug for 6 hours to assess the concentration which killed the tadpoles. Working with a narrower range of concentrations below the lethal one, we then performed dose–response measurements of OCR (Figure 3A and S3B–C) and selected the lowest concentration at which OCR decrease was maximal and beyond which it decreased very little.

Palbociclib stock (LC Laboratories #P-7744) was made at 50 mg/mL in ddH_2O-HCl pH 1 and stored at −20°C[68]. It was then diluted in ddH_2O to a final concentration of 6 µg/mL, unless specified for the dose-response curve (Figure 3A). Ouabain stock was made fresh at 5 mg/mL in ddH_2O and diluted in ddH_2O to a final concentration of 200 µg/mL, unless specified for the dose-response curve (Figure S3C). Torin-1 stock was made at 10 mg/mL in DMSO and stored at −20°C, then diluted to a final concentration of 1 µg/mL (final DMSO concentration was 0.1%) unless specified for the dose-response curve (Figure S3B). Torkinib (PP 242, MedChem Express, #HY-10474) stock was made at 50 µmol/mL in ethanol 100% and stored at −20°C, then diluted to a final concentration of 12.5 nmol/mL (final ethanol concentration was 0.025%), unless specified for the dose-response curve (Figure S3B). Controls comparing the OCR/mass measurement in stage 41 diploids in water or final DMSO or ethanol solvent concentrations confirm that they did not alter the average OCR value in diploids (Figure S3E).

Tail length measurements

Stereoscope images were obtained on a Zeiss® Stereoscope Discovery.V8 with the Leica color camera DNC 2900 and LASX software. Embryos stage 41 or older were transiently immobilized with a low dose of benzocaine (0.008‰ in 1/10X MMR) and placed on 1.5% agarose-coated petri dishes for imaging. Images were analyzed using Fiji software[69].

Microscopy imaging

Confocal imaging was performed on an inverted Zeiss LSM 800 using the Zeiss Zen software, a Plan-Apochromat 20X/0.8 air objective with a pinhole size set at 1 Airy Unit (cell size measurement) or Plan-Apochromat 10X/0.45 air objective with a pinhole opened to the maximum diameter (phospho-histone H3 imaging for tail proliferation assays). For the metaphase spreads, images were acquired using Micromanager 1.4 software[70] on an upright Olympus® BX51 microscope equipped with an ORCA-ER and ORCA-Spark camera (Hamamatsu, Photonics) and Olympus UPlan 60X/NA 1.42 oil objective.

Cell size measurement

Cell areas were manually traced using Fiji software[69]. For each condition, at least 3 clutches and 3–5 embryos per clutch and ploidy were measured.

Model for the relationship between metabolism and cellular maintenance

Previous theoretical work proposed partitioning organism metabolism (B) into two main processes, growth and maintenance[29–31], a model known as the Von Bertalanffy-Richards model of growth[32,33]. Here we propose a slight adaptation of this model to estimate costs of growth and maintenance as a function of ploidy in embryos.

First, we write that:

$$B = \frac{E_S}{m_c}\frac{dm}{dt} + E_d\frac{dN_C}{dt} + B_C N_C \quad (1)$$

where E_S is the cost of synthesis of new units of mass m, m_C is the mass of a cell, with $\frac{dm}{dt}$ equal to the change in mass over time. E_d is the cost of new cell division, $\frac{dN_C}{dt}$ is the rate of cell proliferation, B_C is the basal cellular metabolic rate (maintenance), and N_C the number of cells in the embryo. Note that, compared with previous work in multicellular tissues[29–33], we propose to partition the term “growth” into two distinct processes: biosynthesis and cell cycle progression. Our experimental results show that the latter term does not contribute to metabolic differences across ploidies (Figure 4B). Our experiments also show that maintenance represents nearly half of the energy expenditure at stage 41 (Figure 3E) and is mostly accounted for by the ubiquitous ionic pump Na+/K+ ATPase which maintains plasma membrane potential (Figure 3D–E, Figure 4B). Our model thus focuses on estimating how differences in maintenance may affect the overall metabolic rate.

How does cellular maintenance ($B_C N_C$) change with ploidy? A simple hypothesis is that cellular metabolic rate scales linearly with cell volume. Since cell size measurements suggest a linear scaling between ploidy (P) and cell volume (V_C) in epithelial cells (Figure 1E and F), we can estimate that for an embryo volume V_{embryo}, the number of cells follows:

$$N_C \sim V_{embryo}/V_C \sim 1/P \quad (2)$$

In this case, the product $B_C N_C$ remains constant with ploidy, a result which disagrees with our experimental measurements that OCR decreases with ploidy (Figure 2C). In the alternative hypothesis where cellular metabolic rate remains constant with cell volume, we instead find: $B_C N_C \sim 1/P$. Finally, a third hypothesis is that cellular maintenance scales with cell surface area rather than volume. This is supported by our finding that perturbing membrane stability and ion pumps using DMSO and ouabain abolishes the OCR difference between diploids and triploids (Figure 4B). Importantly, previous work in yeast[12], human stem cells[20], and unicellular organisms[71] also suggested that cellular respiration or metabolic rate increase sub-linearly with cell size (reviewed in[16]). Assuming that metabolic rate scales with surface area, which relates to cell volume to the 2/3 power ($B_C \sim V_C^{2/3} \sim P^{2/3}$), we find:

$$B_c N_c \sim P^{-1/3} \quad (3)$$

To estimate the fraction of the total energy expenditure associated with cell maintenance (φ_M), we turn to our experimental measurements of OCR upon inhibition of biosynthesis (torin-1 and torkinib), cell cycle progression (palbociclib) and membrane potential maintenance (ouabain) which suggest that these processes represent 30 ± 4 %, 26 ± 1 %, and 46 ± 4 % of total embryo energy expenditure, respectively (Figure 3E). Note that the sum of these contribution is 102 ± 4 % (variation calculated by standard error propagation). With the margin of error, the sum is close to 100%, suggesting that these three processes account for the bulk of all relevant energetic costs. Moreover, the estimated cost of membrane potential maintenance by the Na^+/K^+ ATPase is within the range of previously published values[19,72,73].

To estimate the metabolic rate of diploids (B_D), we use equation (1) and write:

$$B_D = (1 - \varphi_m)B_D + B_C N_C \quad (4)$$

Under the assumption that growth and proliferation are constant with ploidy, the metabolic rate of a triploid embryo is thus:

$$B_T = (1 - \varphi_m)B_D + (B_C N_C)_T \quad (5)$$

Under the assumption that cellular metabolic rate scales with surface area as in equation (3), we find:

$$(B_C N_C)_T = P^{-1/3}(B_C N_C)_D = P^{-1/3}\varphi_m B_D$$

Combining equations (5) and (6) and using the experimentally measured φ_M = 46 ± 4 %, the estimated ratio of metabolic rate of triploids over diploids is B_T/B_D = 0.942 ± 0.005. This is in remarkable agreement with our average experimentally measured ratio of 0.94 ± 0.02 in both *X. laevis* and *X. borealis* (Figure S2K).

We note the possibility that some experimentally measured costs might be overestimated due to the fact that embryo cells are not perfectly spherical, and cannot rule out indirect drug effects. Inhibition of biosynthesis, for example, is likely to alter cell cycle progression because of feedback between the two pathways[74] while inhibition of the Na^+/K^+ ATPase by ouabain alters osmolarity in addition to plasma membrane potential[37,38], which may have multiple impacts on cellular physiology including biosynthesis[38,49,75]. These considerations contribute to the uncertainty of the above estimate. Additionally, since torkinib reduces the metabolic difference across ploidies (Figure 4B), future modeling may account for a potential ploidy-dependent cost of biosynthesis. To do so, a crucial question concerns how such costs scale with cell size or surface area. Previous work has shown that growth rate and protein concentration remain constant in cells as ploidy increases for a wide range of cell sizes[49,50] and we have measured that diploid and triploids gain mass at a comparable rate (Figure 1B). It is therefore tempting to hypothesize that the effect of torkinib is instead due to the fraction of protein synthesis that scales with cell surface area (i.e., plasma membrane pumps and proteins[50]), not cell volume. Further studies are needed to test this hypothesis.

QUANTIFICATION AND STATISTICAL ANALYSIS

Statistical analysis—All the analysis and figures were made using R 4.1.2 and the following packages: ggplot2[76], tidyverse[77], dplyr[78], forcats, robustbase and MASS. T-tests in Figures 1D, 2C, 3C, 4A–B and 5C are Welch two samples t-tests. The number of biological replicates and measurements (n) is reported in the figure legend and associated supplementary tables. For all boxplots, the thick line inside the box indicates the mean, and the upper and lower hinges indicate the first and third quartile, the upper and lower whiskers extend from the hinge to the highest (lowest) value within 1.5*IQR (Inter Quantile Range) of the hinge. Data beyond the whiskers are shown as outliers.

Establishing the existence of a power-law relationship between OCR and body mass in embryos—To test the existence of a power-law relationship between OCR and body mass, as reported in adult animals according to Kleiber's law[18], we first focused on diploid *X. laevis* embryos on days 2–5 p.f., which span a significant range in body mass (Figure 2B). We performed linear regressions on the logarithmic or non-transformed values of OCR and body mass. The former gave a higher R^2 (Table S2), indicating that the data was better represented by a power-law relationship in the form: $B = B_0 m^{\alpha}$ (where B is OCR and m is body mass) than by a simple linear relationship (where $B = am + b$). In Figure 2D, we compared this scaling relationship in diploids and triploids from day 3 onwards, because the relationship between OCR and ploidy changes during day 2 (Figures 2C and S2I). While the range of body masses is narrower and the allometric exponent changes a little compared with the one obtained with the full diploid dataset (day 2–5) this analysis reveals different normalization constants B_0 as a function of ploidy (Table S2).

Statistical approach to comparing OCR using bins of mass—The power-law fitting approach described above and in Figure 2B and D is the most rigorous and informative as it allowed us to test the relationship between metabolic rate and body mass and obtain fitted values of B_0. However, this approach requires a large number of single-embryo measurements across a range of masses and can only be used when the regime of scaling between metabolic rate and ploidy is constant, which we verified was qualitatively the case for day 3 to day 5 tadpoles (Figure S2I). Importantly, the power-law fitting approach on day 3 to day 5 *X. laevis* embryos (Figure 2D) concludes that the decrease of B_0 is ~ 5.5 % in triploids compared to diploids. This is in good agreement with the average 6% decrease observed using bins of body mass to compare stage 41 diploid and triploid *X. laevis* or *X. borealis* (Figure S2K), therefore validating the latter statistical approach. Thus, for experiments comparing OCR over narrow ranges of mass (e.g., drug treatment at one specific developmental stage, Figure 3), we used bins of body mass to compare diploid and triploids. Since the power law relates the metabolic rate B (measured by OCR) following: $B = B_0 m^{\alpha}$, the ratio OCR/mass is:

$$\frac{OCR}{m} = \frac{B}{m} = B_0 m^{\beta} \tag{7}$$

where $\beta = \alpha - 1 \approx -0.48$ for embryos measured at day 3 to 5 given the fitted value of α during this period of development (Figure 2B). Therefore, OCR/mass is lower for bins of

higher mass (e.g. see OCR/mass in diploids for the bin 4–5 mg compared with the bin 2–3 mg in Figure 2C).

Supplementary Material

Refer to Web version on PubMed Central for supplementary material.

ACKNOWLEDGEMENTS

We thank the Heald lab for feedback throughout the project, the Harland lab, Helen Willsey, Cameron Exner, and Andrea Wills for *Xenopus* embryo protocols, Christian Erikson for help early in the project, Kelly Miller for sharing cell size measurements in stage 48 *X. longipes* and *X. tropicalis* (see ref.[23]), Van Savage for helpful conversations, Sarina Arain for her availability with OCR-related questions, Youmna Atieh and Xiao Liu for feedback on the manuscript, James K. Utterback for advice on statistical analysis, Anand Varma and Mark Unger for help with imaging *X. longipes* development, and James Evans and the animal facility of UC Berkeley for frog care. R.H was supported by NIH MIRA grant R35GM118183 and the Flora Lamson Hewlett Chair in Biochemistry.

INCLUSION AND DIVERSITY

We support inclusive, diverse, and equitable conduct of research.

REFERENCES

1. Øvrebø JI, and Edgar BA (2018). Polyploidy in tissue homeostasis and regeneration. Development 145, dev156034. [PubMed: 30021843]
2. Storchova Z, and Pellman D (2004). From polyploidy to aneuploidy, genome instability and cancer. Nat. Rev. Mol. Cell Biol 5, 45–54. [PubMed: 14708009]
3. Soltis PS, Marchant DB, Van de Peer Y, and Soltis DE (2015). Polyploidy and genome evolution in plants. Curr. Opin. Genet. Dev 35, 119–125. [PubMed: 26656231]
4. Gibeaux R, Acker R, Kitaoka M, Georgiou G, Van Kruijsbergen I, Ford B, Marcotte EM, Nomura DK, Kwon T, Veenstra GJC, et al. (2018). Paternal chromosome loss and metabolic crisis contribute to hybrid inviability in Xenopus. Nature 553, 337–341. [PubMed: 29320479]
5. Small CD, Davis JP, Crawford BD, and Benfey TJ (2021). Early, nonlethal ploidy and genome size quantification using confocal microscopy in zebrafish embryos. J. Exp. Zool. Part B Mol. Dev. Evol 336, 496–510.
6. Swarup H (1959). The oxygen consumption of diploid and triploid Gasterosteus aculeatus (L). J. Genet 56, 156–160.
7. Atkins ME, and Benfey TJ (2008). Effect of acclimation temperature on routine metabolic rate in triploid salmonids. Comp. Biochem. Physiol. - A Mol. Integr. Physiol 149, 157–161. [PubMed: 18155947]
8. Hermaniuk A, Rybacki M, and Taylor JRE (2017). Metabolic rate of diploid and triploid edible frog Pelophylax esculentus correlates inversely with cell size in tadpoles but not in frogs. Physiol. Biochem. Zool 90, 230–239. [PubMed: 28277949]
9. Sambraus F, Remen M, Olsen RE, Hansen TJ, Waagbø R, Torgersen T, Lock EJ, Imsland A, Fraser TWK, and Fjelldal PG (2018). Changes in water temperature and oxygen: the effect of triploidy on performance and metabolism in large farmed Atlantic salmon. Aquac. Environ. Interact 10, 157–172.
10. Hermaniuk A, Van De Pol ILE, and Verberk WCEP (2021). Are acute and acclimated thermal effects on metabolic rate modulated by cell size? A comparison between diploid and triploid zebrafish larvae. J. Exp. Biol 224.
11. Neumann FR, and Nurse P (2007). Nuclear size control in fission yeast. J. Cell Biol 179, 593–600. [PubMed: 17998401]
12. Yahya G, Menges P, Amponsah PS, Ngandiri DA, Schulz D, Wallek A, Kulak N, Mann M, Cramer P, Savage V, et al. (2022). Sublinear scaling of the cellular proteome with ploidy. Nat. Commun 13, 1–13. [PubMed: 34983933]

13. Hansson KA, Eftestøl E, Bruusgaard JC, Juvkam I, Cramer AW, Malthe-Sørenssen A, Millay DP, and Gundersen K (2020). Myonuclear content regulates cell size with similar scaling properties in mice and humans. Nat. Commun 11, 1–14. [PubMed: 31911652]
14. van de Pol ILE, Hermaniuk A, and Verberk WCEP (2021). Interacting Effects of Cell Size and Temperature on Gene Expression, Growth, Development and Swimming Performance in Larval Zebrafish. Front. Physiol 12, 1–20.
15. Swarup H (1959). Effect of triploid on the body size, general organization and cellular structure in Gasterosteus Aculeatus (L). J. Genet 56, 143–155.
16. Cadart C, and Heald R (2022). Scaling of biosynthesis and metabolism with cell size. Mol. Biol. Cell 33, 1–6.
17. Glazier DS (2009). Metabolic level and size scaling of rates of respiration and growth in unicellular organisms. Funct. Ecol 23, 963–968.
18. Kleiber M (1932). Body size and metabolism. Hilgardia 6, 315–353.
19. Glazier DS (2022). How Metabolic Rate Relates to Cell Size. Biology (Basel). 11, 1106. [PubMed: 35892962]
20. Sagi I, Chia G, Golan-Lev T, Peretz M, Weissbein U, Sui L, Sauer MV, Yanuka O, Egli D, and Benvenisty N (2016). Derivation and differentiation of haploid human embryonic stem cells. Nature 532, 107–111. [PubMed: 26982723]
21. Miettinen TP, and Bjorklund M (2016). Cellular Allometry of Mitochondrial Functionality Establishes the Optimal Cell Size. Dev. Cell 39, 370–382. [PubMed: 27720611]
22. Lengefeld J, Cheng C-W, Maretich P, Blair M, Hagen H, McReynolds MR, Sullivan E, Majors K, Roberts C, Kang JH, et al. (2021). Cell size is a determinant of stem cell potential during aging. Sci. Adv 7, eabk0271. [PubMed: 34767451]
23. Miller KE, Cadart C, and Heald R (2023). Dodecaploid Xenopus longipes provides insight into the emergence of size scaling relationships during development. Curr. Biol 33, 1–10. [PubMed: 36446352]
24. Savage VM, Gillooly JF, Woodruff WH, West GB, Allen AP, Enquist BJ, and Brown JH (2004). The predominance of quarter-power scaling in biology. Funct. Ecol 18, 257–282.
25. Glazier DS (2005). Beyond the “3/4-power law”: Variation in the intra- and interspecific scaling of metabolic rate in animals. Biol. Rev. Camb. Philos. Soc 80, 611–662. [PubMed: 16221332]
26. Savage VM, Allen AP, Brown JH, Gillooly JF, Herman AB, Woodruff WH, and West GB (2007). Scaling of number, size, and metabolic rate of cells with body size in mammals. Proc. Natl. Acad. Sci. U. S. A 104, 4718–4723. [PubMed: 17360590]
27. Mawaribuchi S, Takahashi S, Wada M, Uno Y, Matsuda Y, Kondo M, Fukui A, Takamatsu N, Taira M, and Ito M (2017). Sex chromosome differentiation and the W- and Z-specific loci in Xenopus laevis. Dev. Biol 426, 393–400. [PubMed: 27297884]
28. Mauvais-Jarvis F (2015). Sex differences in metabolic homeostasis, diabetes, and obesity. Biol. Sex Differ 6, 1–9. [PubMed: 25653823]
29. Kempes CP, Dutkiewicz S, and Follows MJ (2012). Growth, metabolic partitioning, and the size of microorganisms. Proc. Natl. Acad. Sci 109, 495–500. [PubMed: 22203990]
30. Brummer AB, and Savage VM (2021). Cancer as a Model System for Testing Metabolic Scaling Theory. Front. Ecol. Evol 9, 691830.
31. West GB, Brown JH, and Enquist BJ (2001). A general model for ontogenetic growth. Nature 413, 628–631. [PubMed: 11675785]
32. Richards FJ (1959). A Flexible Growth Function for Empirical Use. J. Exp. Bot 10, 290–301.
33. Von Bertalanffy L (1957). Quantitative laws in metabolism and growth. Q. Rev. Biol 32, 217–231. [PubMed: 13485376]
34. Rodenfels J, Neugebauer KM, and Howard J (2019). Heat Oscillations Driven by the Embryonic Cell Cycle Reveal the Energetic Costs of Signaling. Dev. Cell 48, 1–13. [PubMed: 30620896]
35. O’Farrell PH (2015). Growing an embryo from a single cell: A hurdle in animal life. Cold Spring Harb. Perspect. Biol 7.

36. Williams MC, Patel JH, Kakebeen AD, and Wills AE (2021). Nutrient availability contributes to a graded refractory period for regeneration in Xenopus tropicalis. Dev. Biol 473, 59–70. [PubMed: 33484704]
37. Silva E, and Soares-da-Silva P (2012). New Insights into the Regulation of Na +,K + -ATPase by Ouabain. In International Review of Cell and Molecular Biology (Academic Press), pp. 99–132.
38. Cadart C, Venkova L, Recho P, Lagomarsino MC, and Piel M (2019). The physics of cell-size regulation across timescales. Nat. Phys 15, 993–1004.
39. Milligan LP, and McBride BW (1985). Energy Costs of Ion Pumping by Animal Tissues. J. Nutr 115, 1374–1382. [PubMed: 2413191]
40. Baker PF, and Connelly CM (1966). Some properties of the external activation site of the sodium pump in crab nerve. J. Physiol 185, 270–297. [PubMed: 16992223]
41. Santos NC, Figueira-Coelho J, Martins-Silva J, and Saldanha C (2003). Multidisciplinary utilization of dimethyl sulfoxide: pharmacological, cellular, and molecular aspects. Biochem. Pharmacol 65, 1035–1041. [PubMed: 12663039]
42. Yu ZW, and Quinn PJ (1998). The modulation of membrane structure and stability by dimethyl sulphoxide. Mol. Membr. Biol 15, 59–68. [PubMed: 9724923]
43. Liedtke HC, Gower DJ, Wilkinson M, and Gomez-Mestre I (2018). Macroevolutionary shift in the size of amphibian genomes and the role of life history and climate. Nat. Ecol. Evol 2, 1792–1799. [PubMed: 30250158]
44. Gardner JD, Laurin M, and Organ CL (2020). The relationship between genome size and metabolic rate in extant vertebrates. Philos. Trans. R. Soc. B Biol. Sci 375, 20190146.
45. Session AM, Uno Y, Kwon T, Chapman JA, Toyoda A, Takahashi S, Fukui A, Hikosaka A, Suzuki A, Kondo M, et al. (2016). Genome evolution in the allotetraploid frog Xenopus laevis. Nature 538, 336–343. [PubMed: 27762356]
46. Evans BJ, Kelley DB, Tinsley RC, Melnick DJ, and Cannatella DC (2004). A mitochondrial DNA phylogeny of African clawed frogs: Phylogeography and implications for polyploid evolution. Mol. Phylogenet. Evol 33, 197–213. [PubMed: 15324848]
47. Gardner JD, Laurin M, and Organ CL (2020). The relationship between genome size and metabolic rate in extant vertebrates. Philos. Trans. R. Soc. B Biol. Sci 375.
48. Rodenfels J, Sartori P, Golfier S, Nagendra K, Neugebauer KM, and Howard J (2020). Contribution of increasing plasma membrane to the energetic cost of early zebrafish embryogenesis. Mol. Biol. Cell 31, 520–526. [PubMed: 32049586]
49. Neurohr GE, Terry RL, Lengefeld J, Bonney M, Brittingham GP, Moretto F, Miettinen TP, Vaites LP, Soares LM, Paulo JA, et al. (2019). Excessive Cell Growth Causes Cytoplasm Dilution And Contributes to Senescence. Cell 176, 1083–1097. [PubMed: 30739799]
50. Lanz MC, Zatulovskiy E, Swaffer MP, Zhang L, Ilerten I, Zhang S, You DS, Marinov G, McAlpine P, Elias JE, et al. (2022). Increasing cell size remodels the proteome and promotes senescence. Mol. Cell 82, 3255–3269.e8. [PubMed: 35987199]
51. Sun SY (2013). MTOR kinase inhibitors as potential cancer therapeutic drugs. Cancer Lett. 340, 1–8. [PubMed: 23792225]
52. Berchtold D, Piccolis M, Chiaruttini N, Riezman I, Riezman H, Roux A, Walther TC, and Loewith R (2012). Plasma membrane stress induces relocalization of Slm proteins and activation of TORC2 to promote sphingolipid synthesis. TL - 14. Nat. Cell Biol 14 VN-r, 542–547. [PubMed: 22504275]
53. Eltschinger S, and Loewith R (2016). TOR Complexes and the Maintenance of Cellular Homeostasis. Trends Cell Biol. 26, 148–159. [PubMed: 26546292]
54. Herst PM, Tan AS, Scarlett DJG, and Berridge MV (2004). Cell surface oxygen consumption by mitochondrial gene knockout cells. Biochim. Biophys. Acta - Bioenerg. 1656, 79–87.
55. Vastag L, Jorgensen P, Peshkin L, Wei R, Rabinowitz JD, and Kirschner MW (2011). Remodeling of the metabolome during early frog development. PLoS One 6.
56. Wessely O, and Tran U (2011). Xenopus pronephros development-past, present, and future. Pediatr. Nephrol 26, 1545–1551. [PubMed: 21499947]
57. Clausen MV, Hilbers F, and Poulsen H (2017). The structure and function of the Na,K-ATPase isoforms in health and disease. Front. Physiol 8, 371. [PubMed: 28634454]

58. White CR, Alton LA, Bywater CL, Lombardi EJ, and Marshall DJ (2022). Metabolic scaling is the product of life-history optimization. Science (80-.). 377, 834–839.
59. Belliveau NM, Chure G, Hueschen CL, Garcia HG, Kondev J, Fisher DS, Theriot JA, and Phillips R (2021). Fundamental limits on the rate of bacterial growth and their influence on proteomic composition. Cell Syst. 12, 924–944.e2. [PubMed: 34214468]
60. Yang X, Heinemann M, Howard J, Huber G, Iyer-Biswas S, Le Treut G, Lynch M, Montooth KL, Needleman DJ, Pigolotti S, et al. (2021). Physical bioenergetics: Energy fluxes, budgets, and constraints in cells. Proc. Natl. Acad. Sci. U. S. A 118, 1–10.
61. Kuznetsova AY, Seget K, Moeller GK, de Pagter MS, de Roos JADM, Dürrbaum M, Kuffer C, Müller S, Zaman GJR, Kloosterman WP, et al. (2015). Chromosomal instability, tolerance of mitotic errors and multidrug resistance are promoted by tetraploidization in human cells. Cell Cycle 14, 2810–2820. [PubMed: 26151317]
62. Storchova Z, and Kuffer C (2008). The consequences of tetraploidy and aneuploidy. J. Cell Sci 121, 3859–3866. [PubMed: 19020304]
63. Gibeaux R, and Heald R (2019). Generation of Xenopus Haploid, Triploid, and Hybrid Embryos. In Vertebrate Embryogenesis: Embryological, Cellular, and Genetic Methods, Pelegri FJ, ed. (Humana, New York), pp. 303–315.
64. Nieuwkoop PD, and Faber J (1994). Normal table of Xenopus laevis (Daudin). A Systematical and Chronological Survey of the Development from the Fertilized Egg till the End of Metamorphosis (Garland Science).
65. Khokha MK, Chung C, Bustamante EL, Gaw LWK, Trott KA, Yeh J, Lim N, Lin JCY, Taverner N, Amaya E, et al. (2002). Techniques and probes for the study of Xenopus tropicalis development. Dev. Dyn 225, 499–510. [PubMed: 12454926]
66. Koller M, Stahel WA, Koller M, and Stahel WA (2011). Sharpening Wald-type inference in robust regression for small samples. Comput. Stat. Data Anal 55, 2504–2515.
67. Lee C, Kieserman E, Gray RS, Park TJ, and Wallingford J (2008). Whole-mount fluorescence immunocytochemistry on Xenopus embryos. Cold Spring Harb. Protoc 3.
68. Duan C, Liu W, Tao Y, Liang F, Chen Y, Xiao X, Zhang G, Chen Y, and Hao C (2022). Two novel palbociclib-resorcinol and palbociclib-orcinol cocrystals with enhanced solubility and dissolution rate. Pharmaceutics 14, 23.
69. Schindelin J, Arganda-Carreras I, Frise E, Kaynig V, Longair M, Pietzsch T, Preibisch S, Rueden C, Saalfeld S, Schmid B, et al. (2012). Fiji: an open-source platform for biological-image analysis. Nat. Methods 2012 97 9, 676–682.
70. Edelstein AD, Tsuchida MA, Amodaj N, Pinkard H, Vale RD, and Stuurman N (2014). Advanced methods of microscope control using μManager software. J. Biol. Methods 1, e10. [PubMed: 25606571]
71. Glazier DS (2009). Metabolic level and size scaling of rates of respiration and growth in unicellular organisms. Funct. Ecol 23, 963–968.
72. Milligan LP, and McBride BW (1985). Energy Costs of Ion Pumping by Animal Tissues. J. Nutr 115, 1374–1382. [PubMed: 2413191]
73. Rolfe DFS, and Brown GC (1997). Cellular energy utilization and molecular origin of standard metabolic rate in mammals. Physiol. Rev 77, 731–758. [PubMed: 9234964]
74. Goranov AI, and Amon A (2010). Growth and division-not a one-way road. Curr. Opin. Cell Biol 22, 795–800. [PubMed: 20667436]
75. Oh S, Lee C, Yang W, Li A, Mukherjee A, Basan M, Ran C, Yin W, Tabin CJ, Fu D, et al. (2022). Protein and lipid mass concentration measurement in tissues by stimulated Raman scattering microscopy. Proc. Natl. Acad. Sci 119, 629543.
76. Wickham H (2016). ggpolt2 Elegant Graphics for Data Analysis (Springer-Verlag New York).
77. Wickham H, Averick M, Bryan J, Chang W, McGowan L, François R, Grolemund G, Hayes A, Henry L, Hester J, et al. (2019). Welcome to the Tidyverse. J. Open Source Softw 4, 1686.
78. Wickham H, François R, Henry L, and Müller K (2018). dplyr: A Grammar of Data Manipulation.

Highlights

- *Xenopus* embryos show a power-law scaling relationship of metabolic rate with mass.
- Triploid embryos have fewer, larger cells than diploids, reducing metabolic rate.
- Energetic costs of the plasma membrane maintenance are lowered in triploid cells.
- Metabolic rate scales with cell size, not genome size across three *Xenopus* species.

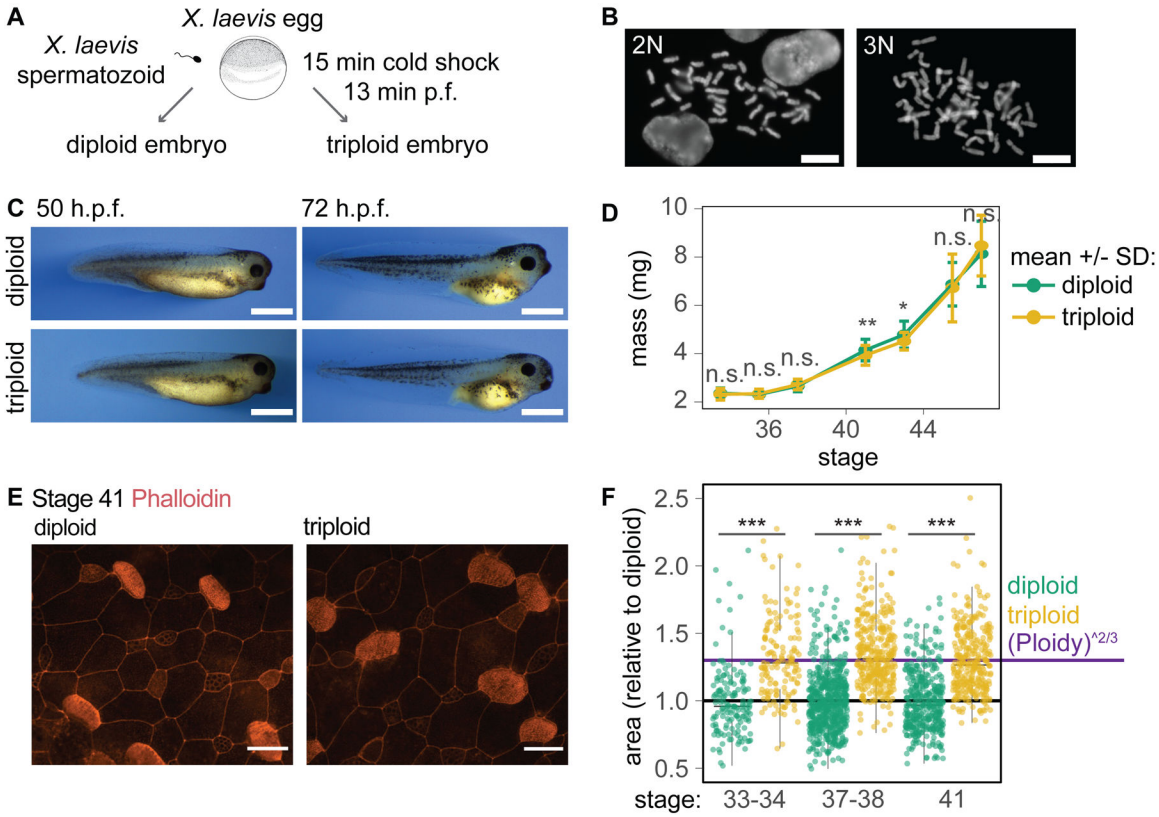

Figure 1. Triploid *X. laevis* develop normally.

(**A**) Triploid *X. laevis* were obtained by blocking polar body extrusion post fertilization (p.f.) using a cold shock. (**B**) The 1.5-fold increase in chromosome number in triploid (3N) compared to diploid (2N) embryos was verified by metaphase chromosome spreads. Scale bar = 10 μm. (**C**) Representative images of diploid and triploid embryos obtained from the same clutch of eggs. Scale bar = 1 mm. (**D**) Compared to diploids, triploids showed a comparable mass increase except for a transient ~ 5% reduction during day 3 (19 clutches, n=10 to 82 embryos per ploidy and stage, details in Table S1). (**E**) TMR-phalloidin staining of actin in ventral epithelial cells of stage 41 diploid and triploid *X. laevis* embryos showing cell outlines and strong actin enrichment at the surface of multiciliated cells. (**F**) Area of diploid and triploid multiciliated cells in embryos at stages 33–34, 37–38 and 41, normalized to diploids of each clutch. (3 clutches, n>150 for each condition). **(D), (F)**, Welch two sample t-test comparing the means, *: p<0.5, **: p<0.01,***: p<0.001. See also Figure S1.

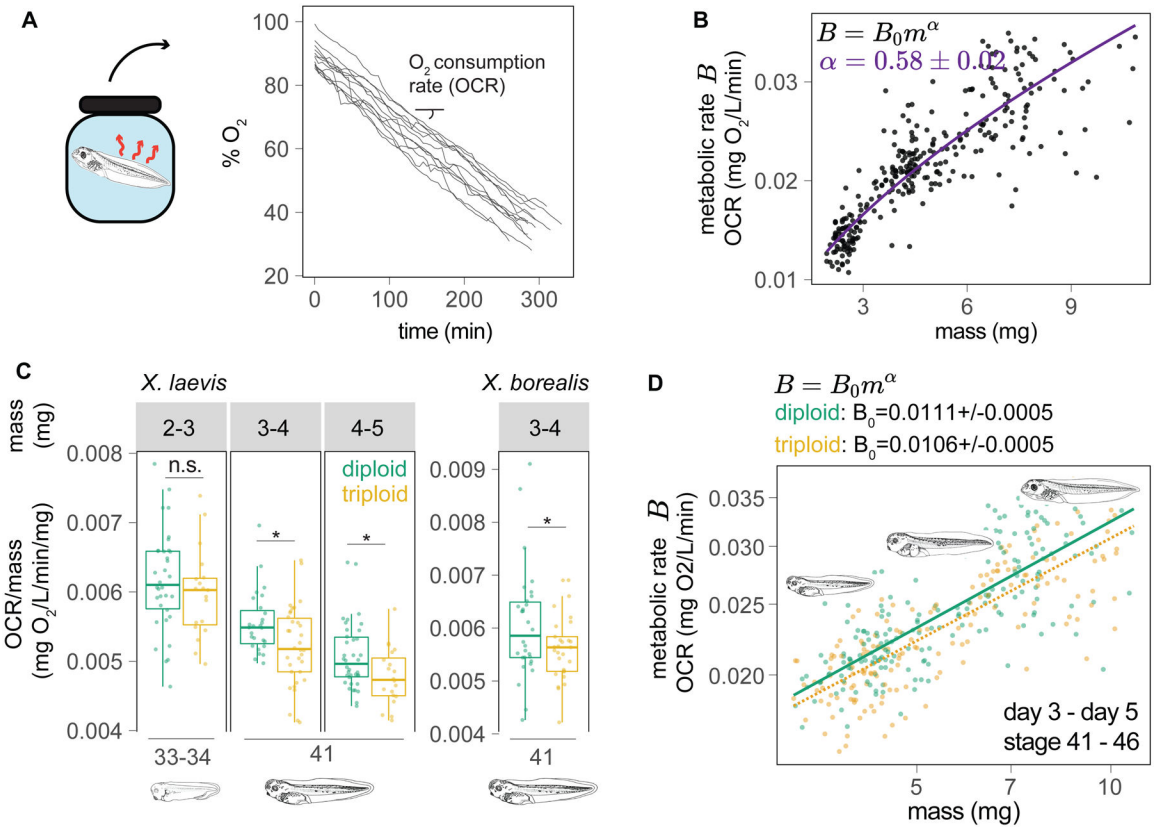

Figure 2. Metabolism assessed by single-tadpole oxygen consumption rates vary between diploids and triploids of both *X. laevis* and *X. borealis*.

(**A**) Single tadpoles were placed in individual glass vials sealed from air. The decrease in O_2 levels over time was used to calculate the oxygen consumption rate (OCR) for each tadpole. (**B**) OCR as a function of body mass in diploid *X. laevis* embryos from day 2 to 5 p.f. The curve shows a fit $B = B_0 m^\alpha$ with values B_0 = 0.0089 ± 0.0002 and α = 0.58 ± 0.02 (n=271) (see Methods and Table S2). (**C**) OCR for bins of body mass and stages in *X. laevis* (left panel) and *X. borealis* (right panel) of diploid and triploid embryos (t-test comparing the means *= p<0.5, **= p<0.01; 3 to 5 clutches per condition, details in Table S3). (**D**) OCR as a function of body mass in diploid (n=189) and triploid (n=165) tadpoles from day 3 (stage 41) to day 5 (stage 46). The lines represent linear fits of the logarithmic values, which yielded the same allometric scaling component exponent α (α = 0.46 ± 0.03), but different Y-intercepts that indicate a lower basal metabolic rate (B_0) in triploids (see Methods and Table S2). See also Figure S2.

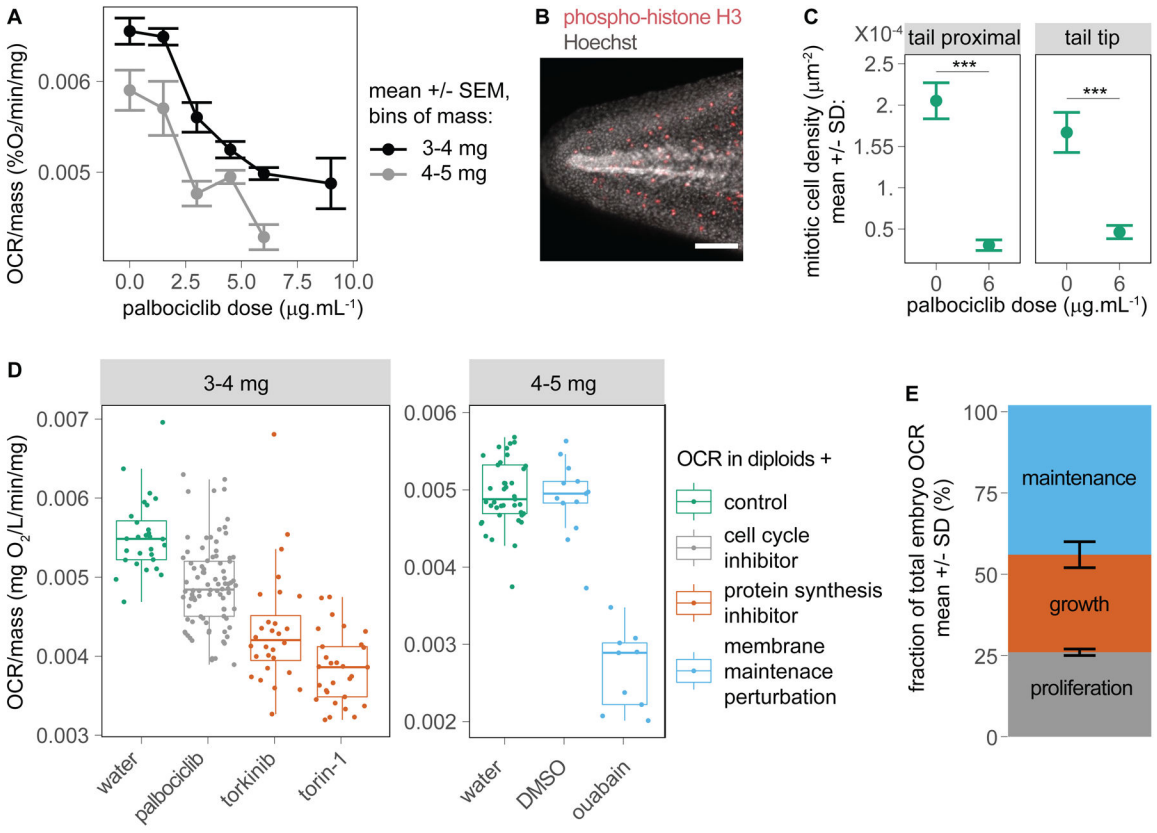

Figure 3. An embryo energy budget establishes the costs of proliferation, biosynthesis, and maintenance.

(A) OCR per mass as a function of palbociclib doses for stage 41 diploid embryos and two bins of mass (6 clutches, n = 2 to 57 per bin of mass and palbociclib concentration). (**B**) Representative image of phospho-histone H3 immunostaining and Hoescht DNA dye staining of tadpole tails (scale bar = 200 µm). **(C)** Mitotic cell density in the tails of stage 41 diploid embryos assessed by quantifying phospho-histone H3-positive cells (n=2, 5–6 embryos per clutch, Welch two samples t-test comparing the means, ***: $p<0.001$). **(D)** OCR per mass for stage 41 diploid embryos in water, 6 µg/mL palbociclib, 12.5 nmol/mL torkinib, 1 µg/mL torin-1, 0.1% DMSO, or 200 µg/mL ouabain. **(E)** The percentage decrease of OCR in diploids upon treatment with drugs in (D) provides an estimate of the contribution of proliferation (palbociclib), growth (torkinib, torin-1), and maintenance (ouabain) to the overall embryo energy expenditure. See also Figure S3 and S4.

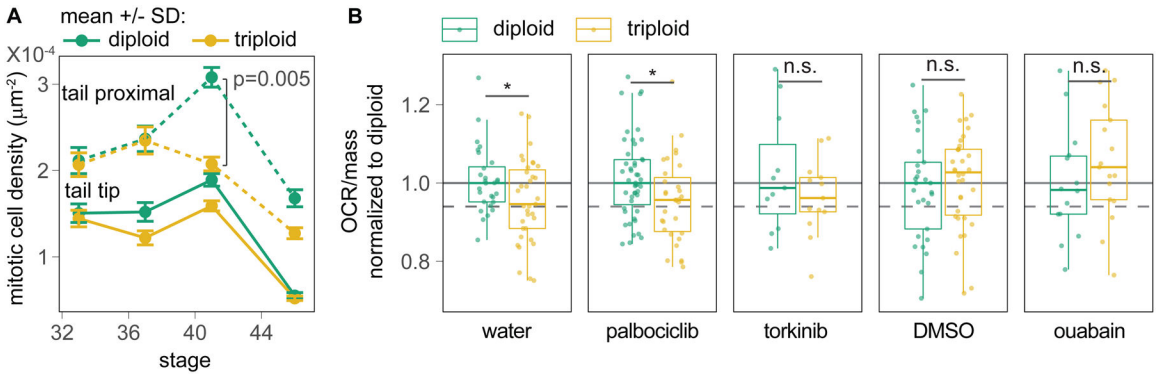

Figure 4. The energetic cost of cell membrane maintenance, not proliferation, accounts for the difference in metabolism between diploids and triploids.

(A) Mitotic cell density in the tails of diploid and triploid embryos assessed by quantifying phosphor-histone H3-positive cells (n=3, 5–6 embryos per clutch) (**B**) OCR per mass normalized to the median diploid value for each condition in stage 41 tadpoles during a 6 hr incubation in water, 6 µg/mL palbociclib, 12.5 nmol/mL torkinib, 0.1% DMSO, or 200 µg/mL ouabain. Results are shown for 3–4 mg embryos except 5–6 mg for ouabain (n=3 to 5 clutches per condition, details in Table S4). Dashed line indicates the average in untreated triploids. **(A), (B),** Welch two samples t-test comparing the means, *: p<0.5, **: p<0.01,***: p<0.001. See also Figure S4.

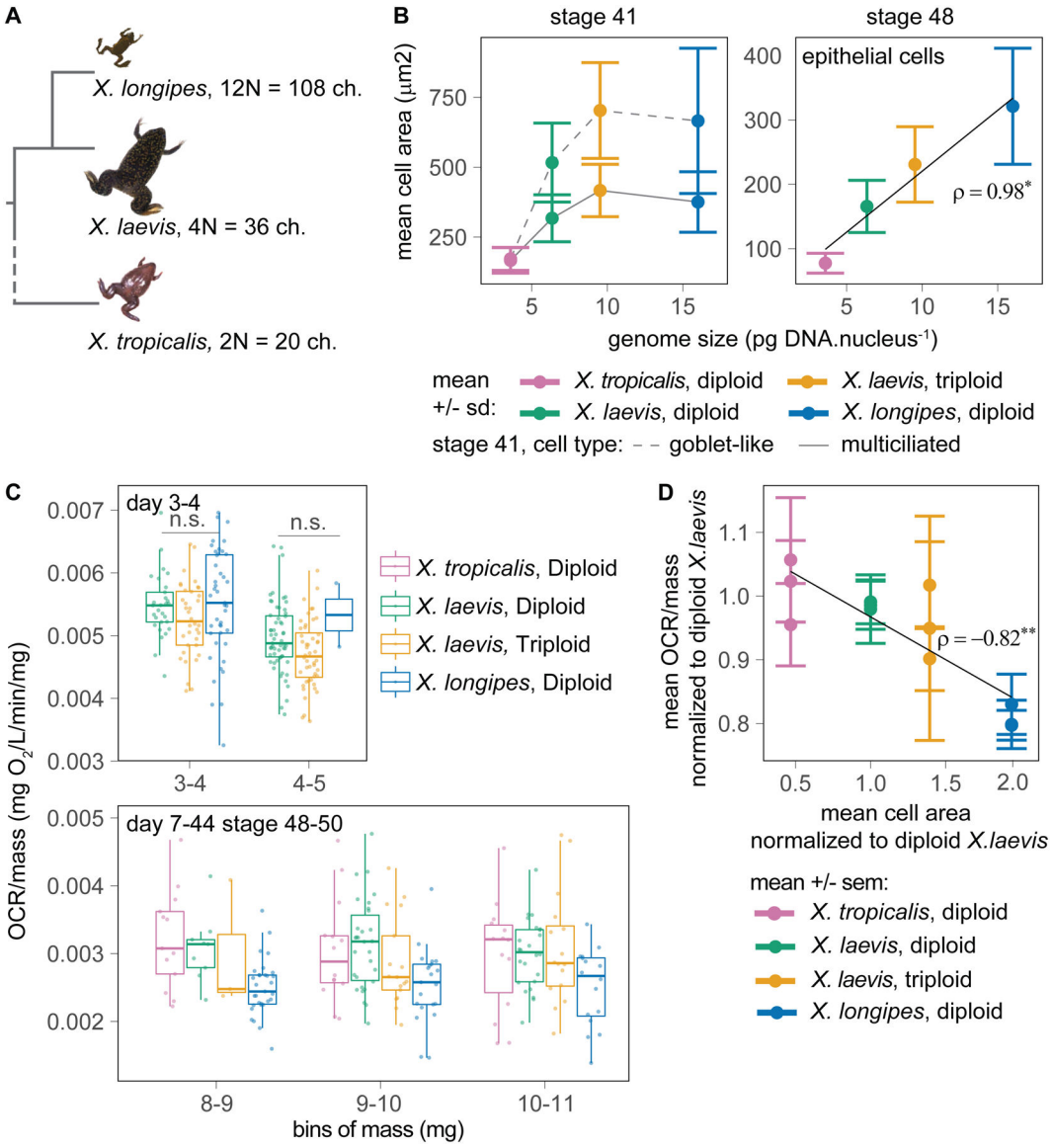

Figure 5: Metabolic rates of *Xenopus* species scale with cell size, not ploidy.

(**A**) *X. longipes, X. laevis* and *X. tropicalis* are 12N, 4N and 2N, respectively, with corresponding differences in chromosome (ch.) number; tree not to scale with phylogenetic distances. (**B**) Cell size measurements show scaling with genome size at stage 48, but not stage 41 (2–5 clutches, n>40 per condition, *X. tropicalis* and *X. longipes* stage 48 data from[23]). (**C**) OCR across species: (top) before the onset of cell size scaling with genome size at day 3–4 (stage 41–46) and (bottom) after scaling onset (stage 48–50) at day 6–8 (*X. laevis*), 7–13 (*X. longipes*), and 26–46 (*X. tropicalis*) (see Table S5 for n of each bin). **(D)** OCR data at stages 48 or later (from Figure 5C, bottom) normalized to the mean *X. laevis* diploid value for each bin of mass (each dot is the value for a different bin of mass and species) and plotted as a function of mean cell area at stage 48 (Figure 5B) normalized to the

X. laevis diploid value. (B) and (D): ρ is the Pearson's correlation coefficient of the means weighted by the SD (*= p value <0.05, **= p value <0.01). See also Figure S2 and S5.

KEY RESOURCES TABLE

REAGENT or RESOURCE	SOURCE	IDENTIFIER
Antibodies		
mouse anti-histone H3 (phosphor Ser10)	Abcam	Cat#: ab 14955 RRID: AB_443110
Alexa Fluor 488 goat-anti mouse IgG (H+L)	Thermo Fisher Scientific	Cat#: A-11001, RRID:AB_2534069
mouse anti ZO-1	Thermo Fisher Scientific	Cat#: 33–9100, RRID:AB_2533147
Chemicals, peptides, and recombinant proteins		
Pregnant mare serum gonadotrophin	Calbiochem	Cat#: 367222
Human chorionic gonadotrophin	Sigma-Aldrich	Cat#: CG10
Sera Micron	Sera	Cat#: 00720
Colchicine	Sigma	Cat#: C9754
Vectashield	Vector Laboratories	Cat#: H-1000–10
Hoescht 33342	Invitrogen	Cat#: H3570
Phusion buffer	New England Biolabs	Cat#: E0553S
Proteinase K	New England Biolabs	Cat#: P8107S
TMR-phalloidin	Thermo Scientific	Cat#: R415
Palbociclib	LC Laboratories	Cat#: P-7744
Ouabain	Sigma Aldrich	Cat#: O3125
torkinib	MedChem Expres	Cat#: #HY-10474
Torin-1	Calbiochem	Cat#: 475991
Critical commercial assays		
Phusion High-Fidelity PCR kit	New England Biolabs	Cat#: E0553S
Experimental models: Organisms/strains		
Xenopus laevis	Nasco	Cat#: LM00535
Xenopus laevis	National *Xenopus* Resource	Cat#: NXR_0031
Xenopus longipes	gift from California Academy of Sciences (San Francisco, CA)	N/A
Xenopus borealis	Nasco	Cat#: LM00698
Xenopus tropicalis	Nasco	Cat#: LM00822
Xenopus tropicalis	National *Xenopus* Resource	Cat#: NXR_1018
Oligonucleotides		
Primers (*X. laevis* W3 gene sequence amplification), Forward: AAAACCATGACCTCCCGGATAC Reverse: TAGGGAGGGGTTTGGAGGTTC	Mawaribuchi et al.[27]	N/A
Software and algorithms		
Presens Software	Presens	N/A
R (4.1.2), packages ggplot2, tidyverse, dplyr	Wickham et al.[76–78]	https://www.r-project.org/
Micromanager (1.4)	Edelstein et al.[70]	N/A
FIJI (2.1.0/1.53s)	Schindelin et al.[69]	https://imagej.net/software/fiji/
Other		

REAGENT or RESOURCE	SOURCE	IDENTIFIER
Mettler Toledo Excellence XSR Analytical Balance	Mettler Toledo	Cat#: XST105DU
Oxygen Sensor Dish Reader v4	Presens	Cat#: 200001059
1mL SensorVials	Presens	N/A (custom-made)
2mL SensorVials	Presens	Cat#: 200001798
4mL SensorVials	Presens	Cat#: 200001369